ADVANCED MATERIALS
www.advmat.de

Piezotronic Effect in Flexible Thin-film Based Devices

*Xiaonan Wen, Wenzhuo Wu, Yong Ding, and Zhong Lin Wang**

Piezoelectric ceramics with large piezoelectric coefficients such as $Pb(Zr_xTi_{1-x})O_3$ (PZT) have been conventionally utilized for applications in electromechanical sensors, actuators and energy harvesters.[1,2] PZT, however, is electrically-insulating and hence less useful for building electronic devices. Recently, Wurtzite-structured piezoelectric semiconductors such as ZnO, GaN, InN and ZnS have attracted intensive attentions due to their potentials in realizing novel applications by conjunction of piezoelectric effect in electronic transport.[3–6] Piezoelectric-polarization-induced piezopotential in strained piezoelectric semiconductors is capable of modulating carrier transport across the barriers/junctions,[7] leading to a new mechanism for regulating charge carrier transport in addition to the well-known electrically-induced 'field-effect'.[8] This modulating effect on charge carrier transport due to coupling between piezoelectricity and semiconducting property is known as the *piezotronic effect*,[7–11] and has triggered numerous studies ever since its discovery in 2006, unfolding its potentials in enabling novel applications for sensors, flexible electronics, optoelectronics, smart MEMS/NEMS and human–machine interfacing.[12–18]

Currently, almost all of the demonstrated piezotronic devices are based on one dimensional (1D) Wurtzite nanostructures, mostly ZnO nanowires (NWs). Although 1D nanostructures are promising building blocks for future electronics, technical difficulties in implementing 1D nanostructures-based devices hinder their immediate applications. Despite that numerous techniques have been reported for bottom-up synthesis of 1D semiconductor nanostructures, the lack of uniformity in as-synthesized materials, in terms of dimensions, morphologies and doping levels, leads to performance inconsistency from device to device.[19–21] Moreover, the techniques currently available for positioning, aligning and integrating as-synthesized 1D nanostructures are either cumbersome or incompatible with state-of-art microfabrication processes.[22,23] Specifically for piezotronic applications, in addition to feasibly integrating 1D nanostructures with microfabrication of device architectures and peripheral circuits, determination and engineering control of the polar *c*-axis orientation in as-synthesized nanomaterials, which still remains elusive, is of pivotal importance for further construction of integrated devices/systems. On the other hand, piezotronic effect is prospected to be a pervasive effect[7,24] and it is hence not only natural but also beneficial to investigate and utilize piezotronic effect in thin film based material systems, potentially circumventing the limitations posed by 1D nanostructures and fully appreciating the state-of-art microfabrication technologies.

The success of semiconductor technology, which has led to advancement of modern electronics and optoelectronics over the past few decades,[25,26] is enabled by thin-film processing that provides engineering control over material properties as well as scalable integrated fabrication processes. Considering the technological compatibility, piezoelectric semiconductor thin films could be the excellent alternative to 1D counterpart for realizing piezotronic applications. Various methods exist for growing piezoelectric semiconductor thin films, such as physical vapor deposition,[27,28] wet chemical deposition,[29,30] radio frequency (RF) sputtering,[31,32] molecular beam epitaxy[33,34] and metalorganic chemical deposition.[35,36] For applications like electromechancial sensing and human-machine-interfacing, flexible polymer substrates and hence compatible low-temperature growth of active materials are required, which renders direct epitaxial growth of single-crystalline thin film difficult. The presence of piezoelectricity does not necessarily rely on single-crystallinity, but rather requires the alignment of polar axis of the grains, which is also achievable in poly-crystalline films deposited by non-epitaxial techniques due to self-texturing phenomena and lack of center of symmetry in the as-deposited textured structures.[37–39] Taking into account of factors such as growth uniformity, reproducibility, process compatibility and scalability, RF sputtering is the technique of choice for our investigations on thin film based piezotronic effect and related potential applications.

Here, we report the first study of piezotronic effect in RF-sputtered semiconductor thin films. The structural properties of engineered ZnO thin film in this work are characterized before further integrating it into functional piezotronic devices. Modulation of charge carrier transport via piezotronic effect is successfully demonstrated in these thin film based devices, and the underlying mechanism is also discussed. Moreover, the tuning effect of strain-induced piezopotential on the UV sensing capability of thin-film piezotronic device has been investigated. This study shows the possibility of building thin film based piezotronic devices for technological applications.

First, ZnO thin film with controllable property was grown via RF sputtering on flexible PET substrates for structure analysis. Parameters such as chamber pressure, sputtering power, mixing ratio of gases as well as sputtering temperature are manipulated systematically to achieve optimized piezoelectric characteristics and charge carrier density of the sputtered ZnO thin film. Specifically, the chamber pressure and sputtering power were set at 12 mTorr and 125 W respectively to achieve a reasonable growth rate. The sample holder was heated up to

X. N. Wen, W. Z. Wu, Dr. Y. Ding, Prof. Z. L. Wang
School of Materials Science and Engineering
Georgia Institute of Technology
Atlanta, Georgia 30332-0245, USA
E-mail: zlwang@gatech.edu
Prof. Z. L. Wang
Beijing Institue of Nanoenergy and Nanosystems
Chinese Academy of Sciences
Beijing, China

DOI: 10.1002/adma.201300296

ADVANCED MATERIALS
www.advmat.de

Materials Views
www.MaterialsViews.com

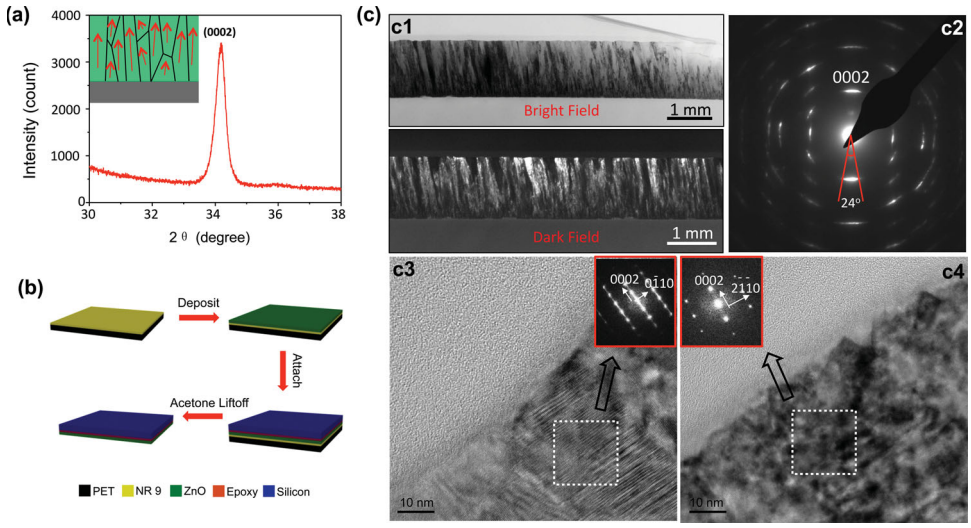

Figure 1. Structure characterization of the polycrystalline ZnO thin film grown by RF sputtering onto PET substrates. (a) XRD diffraction spectrum of the ZnO thin film. (b) Schematics on how to transfer the as-sputtered ZnO thin film from PET to silicon for TEM sample preparation. (c) TEM characterization results. c1 shows the bright field and dark field cross-sectional TEM image of the thin film. (c2) shows the diffraction pattern of the thin film. (c3) shows the HRTEM images of two different locations along the boundary. The corresponding diffraction patterns are shown in the insets.

100 °C during the growth process to improve crystallinity of the as-sputtered film. Finally, the as-grown ZnO thin film was treated with oxygen plasma before electrode fabrication for improved electrical contacts. The dominant diffraction peak in X-ray diffraction (XRD) result (**Figure 1**a) for the as-grown film centers around $2\theta = 34.3°$, which corresponds to the (0002) plane of Wurtzite ZnO. The other observable diffraction peak within the range of (25°, 40°) is the ($10\ \bar{1}1$) peak arising from non-equilibrium growth. This result indicates that <0001>, corresponding to the *c*-axis of Wurtzite ZnO, is the preferred growth direction and suggests that the as-grown film consists of multiple mesoscopic columnar grains. As is schematically shown in the inset of Figure 1a, alignment of the *c*-axes within these columnar grains gives rise to macroscopically observed piezoelectricity of the ZnO polycrystalline thin film. To obtain further in-depth structural analysis, the ZnO thin film sputtered on flexible substrates (PET in our case) was examined using transmission electron microscopy (TEM). The incompatibility of flexible substrates for cross-section TEM sample preparation was overcome by introducing a transfer technique as described in Figure 1(b). A sacrificial layer of photoresist (NR9) was spin-coated onto the PET substrate before the subsequent growth of ZnO thin film, with the sputtering parameters specified above. A silicon substrate was attached to the as-grown ZnO film with epoxy gel and the sample was then baked at 85 C° for an hour to improve epoxy's resistance to solvents. Lastly, the sample was put into acetone to dissolve the sacrificial layer and the ZnO thin film was successfully transferred from PET substrate to silicon substrate, which is compatible with TEM sample preparation. The TEM characterization results are shown in Figure 1(c). Bright field and dark field cross-sectional TEM images of the transferred ZnO thin film are shown in Figure 1(c1), confirming the columnar-grain structure of as-sputtered film. Electron diffraction pattern is shown in Figure 1(c2) and the arc-shaped diffraction spot of (0002) further proves the alignment of *c*-axes among the columnar grains of the as-grown ZnO thin film. The 24° spread angle of the spot relative to the center of the pattern indicates that most grains have their *c*-axes lie within the range of -12°~12° relative to the normal direction of the substrate. Figure 1(c3) and Figure 1(c4) present high resolution TEM (HRTEM) images at two different locations along the boundary, clearly showing that the *c*-planes are generally parallel to the boundary for both grains. In addition, from the diffraction pattern in the two insets, it can be seen that while their *c*-axes are aligned along the same direction, there is a 30° in-plane rotation relative to each other. This implies that the as-sputtered film has no preferred crystal orientation in directions perpendicular to the overall effective *c*-axis, which leads to the cancellation of the overall piezoelectric effects perpendicular to the *c*-axis. These results discussed above fully support the conclusion that the as-sputtered ZnO thin film on PET substrates has columnar grains with preferred *c*-axis orientation and thus is piezoelectric.

In order to conclude the polarity of the corresponding electric field, the *polarity* of the film needs to be determined. Here, piezoelectric tests were performed for this purpose, by investigating the strain-induced electrical outputs of as-assembled device, which has the metal-ZnO thin film-metal structure. A layer of 5 nm chromium (Cr) was deposited onto PET first by electron-beam evaporation to serve as the bottom electrode and adhesion layer. Then part of the Cr layer was masked and ZnO thin film was subsequently grown on selectively-exposed region of the Cr layer by RF sputtering. Finally, a layer of 5 nm Cr top electrode was deposited on ZnO thin film. The device was then connected to a voltage pre-amplifier, firstly with the top side of the device connected to the positive pole, as sketched in **Figure 2**a. The linear actuator was programmed to apply mechanical strains by periodically pushing, holding and releasing the device while corresponding electrical outputs from device were acquired. As can be seen from the typical voltage signals generated by the device upon straining (Figure 2a), when the device was pushed by the actuator, ZnO thin film

Adv. Mater. **2013**,
DOI: 10.1002/adma.201300296

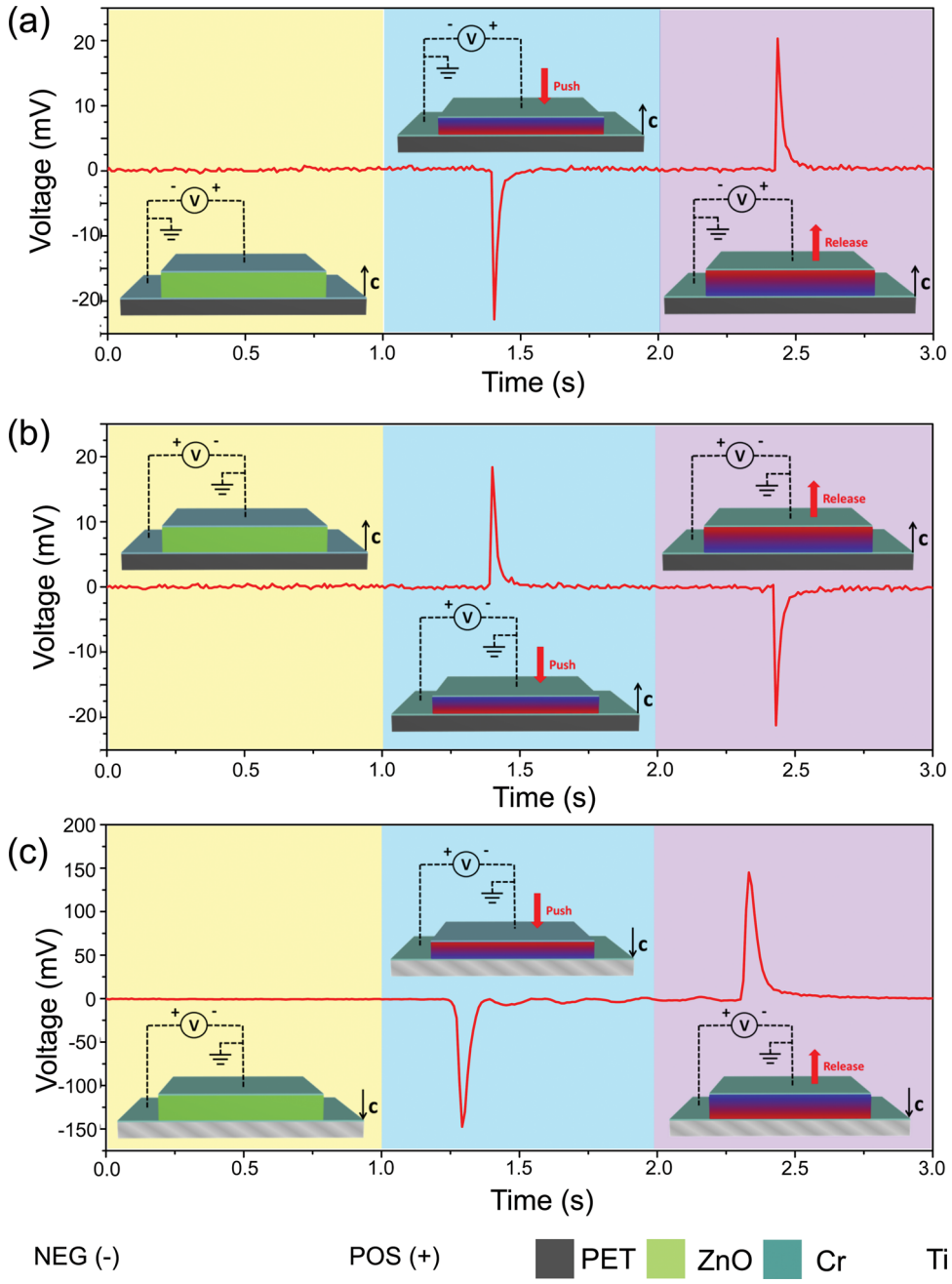

Figure 2. Piezoelectric tests were performed to determine the *c*-axis orientation of the ZnO piezoelectric thin film. The color gradient at the bottom represents the distribution of piezopotential. (a), (b) Test was performed on PET based samples with top electrode each connected to the positive pole of voltage pre-amplifier in (a) and negative pole of voltage pre-amplifier in (b). The sequence of electric pulses indicates that *c*-axis of the as-grown film is pointing up and away from the PET/ZnO interface. (c) Control test was performed by replacing the PET substrate with titanium foil and top electrode connected to the negative pole of voltage pre-amplifier. The sequence of electric pulses indicates that *c*-axis of the as-grown film is pointing down towards the Ti/ZnO interface, opposite to that grown on PET substrates.

was subject to compressive strain and a negative electric pulse was recorded. After holding the sample for 1 s, the pressing force was released and a positive electric pulse can be observed. Since positive piezopotential occurs at the positive side of *c*-axis when ZnO is under tensile strain and negative piezopotential occurs at positive side of *c*-axis when ZnO is under compressive strain, the above observed results indicate that *c*-axis of the as-sputtered ZnO thin film grown on PET substrate is pointing up and away from the PET/ZnO interface (Figure 2a). To verify this, connection to the two poles of voltage-preamplifier was switched and it can be seen from Figure 2b that a positive pulse was generated upon pushing and a negative pulse was observed upon releasing the sample, which is consistent with the above conclusion. A control test was also performed by replacing the

PET substrate with titanium foil while maintaining all other parameters unchanged. By comparing the results obtained from control group in Figure 2c with those in Figure 2b, it can be concluded that as-sputtered ZnO thin film grown on titanium foil possesses the opposite *c*-axis polarity to that grown on PET substrate, with its *c*-axis pointing down towards the Ti/ZnO interface. This set of results implies that properties of the substrates are crucial in dictating the piezoelectric polarity of the RF-sputtered ZnO thin film, which can be explained from two aspects: heat is generated and transferred to the substrate during the sputtering process; positive charges are transferred from positive argon ions in the chamber atmosphere to the substrate through collision. Previous studies also suggested that thermal conductivity and electric conductivity of the underneath substrate material can affect the piezoelectric polarity of the as-grown film effectively.[40,41] For the case of PET substrates, although a grounding electrode is used, it cannot dissipate heat and transfer electric charges efficiently due to the fact that the grounding electrode is only 5 nm thick and is isolated both thermally and electrically from the metal sample holder by the underneath 500-μm-thick PET substrate. Consequently, during the initial stage of ZnO film growth, heat and positive charges will accumulate on the substrate surface, both making adsorption of oxygen atoms more energetically favorable than that of zinc atoms. This initial stacking sequence dictates that *c*-axis of the as-grown film is pointing up from the interface. For the case of titanium foils, on the other hand, conductivities for heat and electricity are both much higher and the zinc atom layer with higher surface energy will hence tend to be adsorbed first while the oxygen atom layer with lower surface energy will tend to terminate the growth, leading to the reverse polarity orientation in which *c*-axis points down towards the interface. However, polarity control of the as-sputtered piezoelectric film is complex and non-trivial in the sense that it's not only influenced by substrate properties but also sputtering conditions and many other factors, which needs more in-depth investigations.

Based on the above characterization results, the feasibility of as-grown ZnO film for piezotronic applications has also been investigated. ZnO piezoelectric thin film was directly grown onto PET substrates with identical process parameters. A pair of top electrodes was made subsequently by electron-beam evaporation, each with size of $1mm^2$ in the shape of square and separated from each other by 500 μm. In addition to piezotronic effect, several other conventionally well-known mechanisms may also contribute to the observed conductivity change of the device. One is the geometrical effect which can be quantitatively expressed as $R = \rho l/A$, and change in material dimensions will lead to resistance change. The other is the piezoresistive effect that arises from change of inter-atomic spacing due to external strain, leading to change in bandgaps. It is worth noting that these two effects are both 'volume' effects and only depend on bulk properties of the semiconductor material while piezotronic effect modulates the material conductivity by affecting characteristics of metal-semiconductor interface.

In order to determine which mechanism dominates in the as-fabricated ZnO thin film device, a pair of Ti/Au (5 nm/ 25 nm) electrodes was deposited sequentially onto the first group of ZnO thin films in order to form Ohmic contacts with ZnO. Due to the high carrier density near junction interface associated with Ohmic contact, the effect of piezopotential can be significantly mitigated,[42] while the contributions in conductivity change due to geometrical and piezoresistive effects should remain unaffected. *I-V* characteristics were subsequently obtained when the device was subject to different strains and the results shown in **Figure 3**a indicate that for strain up to ±0.48%, both geometrical and piezoresistive effects have little influence on the device conductivity. The stress states introduced here in the film is different from the one used in the piezoelectric test, but both stress states will lead to strains in the overall effective polar direction of the ZnO thin film, which is perpendicular to the substrate. Strain values are estimated according to analytical solutions for elastic bending provided by previous studies,[43] with tensile strain defined as positive and compressive strain defined as negative. The strain values used here are for longitudinal strains induced parallel to the substrate plane, which is for calibration purpose. The transverse strains in the films, which are along the overall effective polar direction of the ZnO thin film, can be estimated accordingly (using properties of film such as Poisson's ratio).

In the second group of devices, 30 nm Au was used instead as the electrodes (namely source and drain electrodes) to form Schottky contacts with ZnO, which was confirmed by the *I-V* curves shown in Figure 3b. When a compressive strain was applied, current flowing through the device increased; when a tensile strain was applied, current flowing through the device decreased. To explicitly demonstrate the "*gating*" effect of external strain on modulating the charge carrier transport in ZnO thin film piezotronic device, current values (I) in device under various strains were monitored at fixed bias. I_0 was the current flowing through the device when no strain was applied. As can be seen from the I/I_0-strain curve in Figure 3c, the currents in the device corresponding to each strain applied were similar when either the source or drain electrode was reversely biased (red triangles for 10 V bias on source and green circles for 10 V bias on drain). The slight difference observed might be caused by unintentionally introduced variations in the Schottky contacts at source and drain electrodes during fabrication.

The strain-induced change of Schottky barrier height (SBH) is also calculated[24,44] and plotted in Figure 3c by utilizing the thermionic emission-diffusion theory, presenting a change of 60 meV in SBH at both contacts when the change of applied strain was 1%. The temporal-domain current response to applied periodic strains is then shown in Figure 3d, demonstrating the feasibility of utilizing ZnO thin film piezotronic devices as electromechanical sensors with decent reliability. To further characterize uniformity and reliability of our devices' operation, 100 of such devices are fabricated and their current values at 2 V bias and zero strain are collected. As summarized in Figure 3e (histogram in blue), 85% of the devices have current values within the range of 2 ± 0.2 μA, with the mean value of 2.065 μA and standard deviation of 0.172 μA. It is worth noting that under 2 V bias, the current flowing through our device is increased by ~14 μA under a compressive strain of -0.36% and decreased by ~1.8 μA under a tensile strain of 0.72%, both significantly larger than the standard deviation observed. This suggests the good uniformity and reliable operation of our thin-film based piezotronic devices. Cyclic bending

Adv. Mater. **2013**,
DOI: 10.1002/adma.201300296

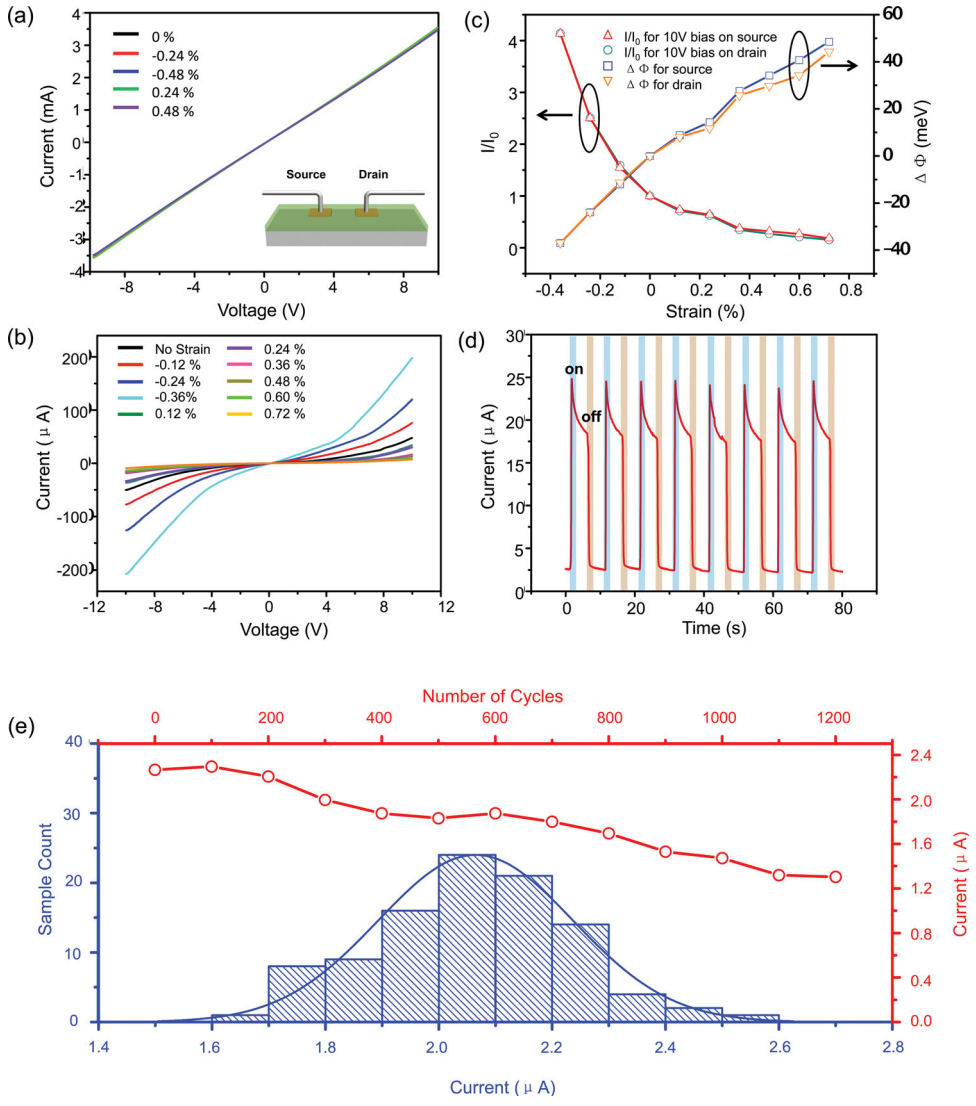

Figure 3. (a) *I-V* curves under different strain values were obtained from a device with Ohmic contact electrodes, indicating that both geometrical and piezoresistive effects have little influence on the device resistance for strains up to ±0.48%. The inset is a schematic of the device. (b) *I-V* curves under different strains were obtained from a device with Schottky contact electrodes, demonstrating modulation of charge carrier transport via piezotronic effect. (c) Calculated changes in current and SBHs explicitly demonstrate the "*gating*" effect of external strain on charge carrier transport in ZnO thin film piezotronic device. (d) Temporal-domain current response to applied periodic strains presents the feasibility for electromechanical sensing applications with decent reliability. (e) Uniformity is demonstrated by collecting current values of 100 devices, shown in the blue histogram; fatigue behavior is investigated with cyclic bending test, shown in the red curve.

test is also performed to investigate the fatigue behavior of our devices. A relatively large compressive strain of -2.5% (corresponding to a bending radius of 1.5 cm) is periodically applied onto the device to accelerate the aging process and the current values under 2 V are recorded per 100 bending cycles. From the results shown in Figure 3e (red curve), it can be seen that the initial current value is 2.26 μA and then gradually drops to 1.31 μA after 1200 bending cycles. This level of current decrease from fatigue is also much smaller than the variations induced by piezotronic effect, indicating stability and reliability in operation of our devices even under cyclic bending with large magnitude of induced strain.

The band diagrams of ZnO thin film piezotronic devices are illustrated in **Figure 4** to better demonstrate the underlying working mechanism. Figure 4a shows the Schottky barriers formed at both contacts with similar barrier heights. When the device is connected to an external power source, the quasi-Fermi level of one electrode is raised (source side here), giving rise to the band diagram shown in Figure 4b, which, however, does not affect the barrier heights from the metal sides on both electrodes. When a tensile strain is applied to the device, negative piezoelectric polarization charges are induced at the top surface of ZnO film. These immobile ionic charges deplete free electrons near the metal-semiconductor interface and therefore

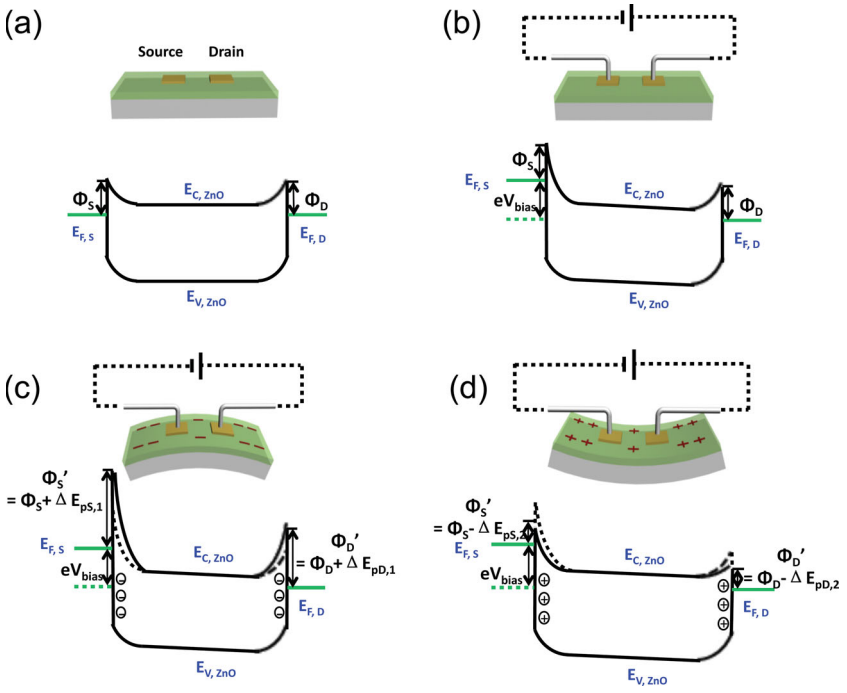

Figure 4. Band diagrams of ZnO thin film piezotronic devices, illustrating the underlying working mechanism. (a) Schottky barriers form at both contacts with similar barrier heights. (b) The quasi-Fermi level of one electrode is raised (source side here) when the device is connected to an external power source. (c) When tensile strain is applied to the device, negative piezoelectric polarization charges are induced at the top surface of ZnO film, depleting free electrons near the metal-semiconductor interface and increasing the SBHs at both contacts. (d) When compressive strain is applied to the device, positive piezoelectric polarization charges are induced at the top surface of ZnO film, attracting free electrons towards the metal-semiconductor interface and decreasing the SBHs at both contacts.

increase the SBHs at both contacts, as shown in Figure 4c. When a compressive strain is applied to the device, on the other hand, positive piezoelectric polarization charges are induced near the top surface of the ZnO film, attracting free electrons towards the metal-semiconductor interface and therefore decreasing the SBHs at both contacts, as shown in Figure 4d. The conductivity of the entire thin film device is dictated by the reversely biased contact and the effective conductivity of the device is sensitive to the change in SBH at that specific contact. Different from piezotronic devices based on 1D nanomaterials in which metal-semiconductor contacts are formed at the two opposite polar surfaces, both source and drain electrodes in the ZnO thin film piezotronic devices are in contact with the same surface of as-deposited ZnO film, and hence piezoelectric polarization charges with same polarity will be induced at both Schottky contacts when external strain is applied. This leads to the observed *I-V* curves (Figure 3b) in which same tuning trend of applied strain can be observed when either source or drain side is reversely biased. As pointed out earlier, this helps circumvent the difficult and elusive predetermination of *c*-axis orientation for 1D nanostructures and brings significant simplification and convenience for further construction of integrated devices/systems.

Finally, ZnO piezotronic thin film based UV sensor was demonstrated and the feasibility of modulating its UV sensing capability by externally applied strain has been investigated. A 365-nm UV lamp was used in the experiment. For each test, UV light was turned on for 1 s and then switched off, while the temporal response of current from the device was monitored under bias of 5 V. In **Figure 5**a, the black curve was recorded when no strain was applied to the device, showing a sensitivity (defined as the percentage increase of current values) of 25% and a reset time of ~880 s. When 0.24% tensile strain was applied, an apparent enhancement of sensitivity was observed, from 25% to 89.25% with a shorter reset time of 582 s, as shown by the blue curve. When the applied tensile strain was increased to 0.48% (the red curve), the UV sensitivity further increased to as high as 112.5% with an even shorter reset time of 337 s. The cases for device under compressive strains are also obtained and plotted in Figure 5b for comparison. When -0.24% compressive strain was applied, the device sensitivity decreased from 25% to 13.21% (green line). As the applied compressive strain was increased to -0.48%, as shown by the orange curve, the sensitivity further decreased to 12.9%. The corresponding reset time increased to over half an hour for both cases. The tuning effect of strain on device's UV sensitivity is summarized in Figure 5c and a significant enhancement of sensitivity by applying tensile strain can be observed.

In addition to the direct contribution from photon-generated excess carriers, ZnO has another important mechanism[45–47] that contributes to its UV sensing capability. In dark environment, oxygen can be adsorbed onto ZnO surface through the reaction [$O_2 + e^- \rightarrow O_2^-$]. Since free electrons are consumed by this adsorption, a depletion layer is consequently created that decreases the conductivity near the film surface. Upon UV illumination, excess electron-hole pairs will be generated and

Adv. Mater. **2013**,
DOI: 10.1002/adma.201300296

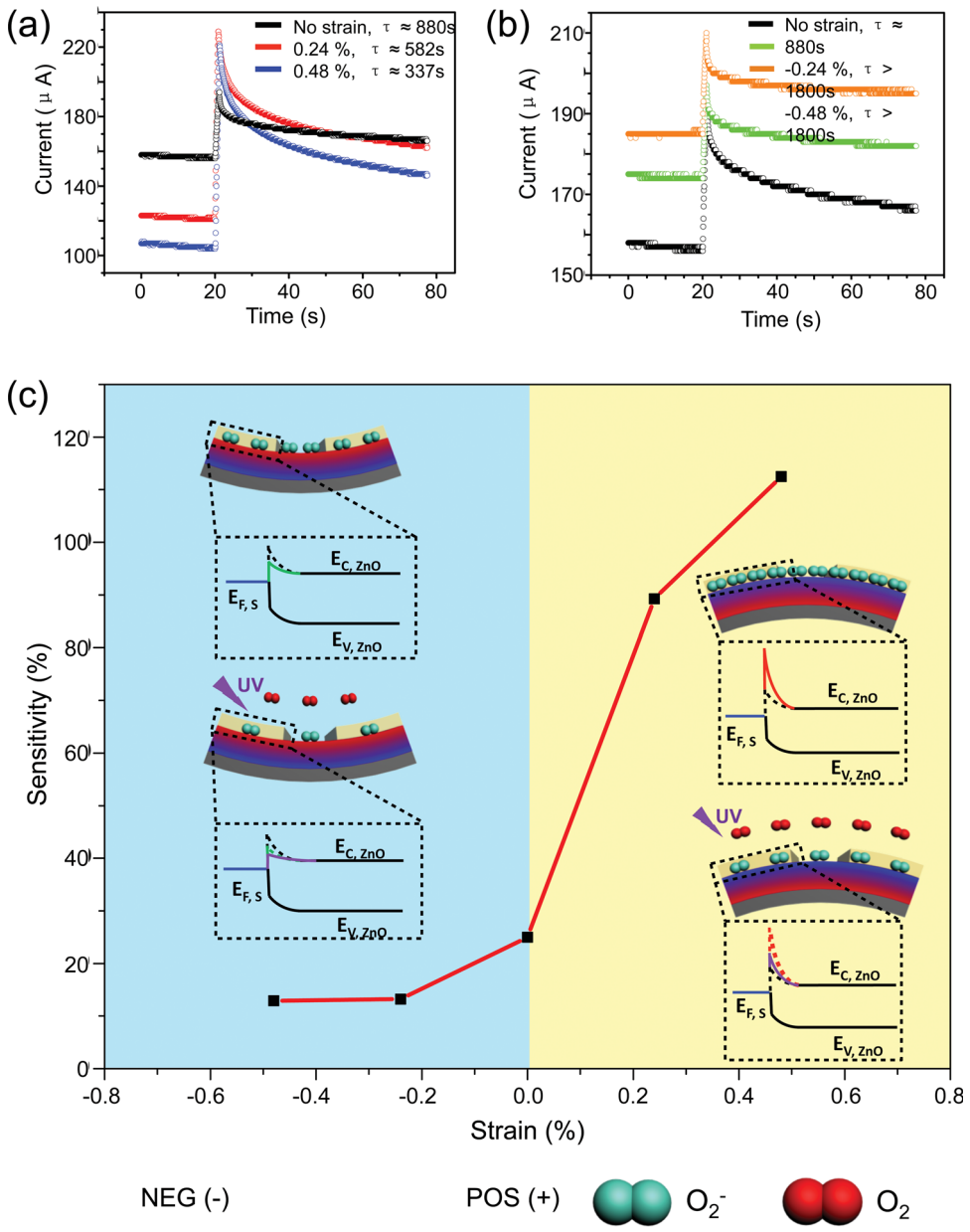

Figure 5. ZnO piezotronic thin film based UV sensor with tunable sensing capability. The color gradient at the bottom represents the strain induced piezopotential. (a) Tensile strains are applied to the device which increases the UV sensitivity and decreases the reset time. (b) Compressive strains are applied to the device which decreases the UV sensitivity and increases the reset time. (c) Sensitivity of the UV sensor under different strain values. The insets explain the underlying mechanism of the strain tuning effect.

the generated holes can discharge the adsorbed oxygen ions, leading to the increase of surface conductivity. Meanwhile, with the accumulation of excess electrons, oxygen will be re-adsorbed and finally a new equilibrium is reached. When the illumination is turned off, electrons and holes will start to recombine with each other. This recombination process can, however, be very slow due to the hole trapping effects at the surface, mitigating the re-adsorption of oxygen, which explains the long reset time normally observed in ZnO based UV sensors.[45] The above mechanism applies to the situation where bare ZnO is exposed to UV light. For our device, in addition to the above processes, the Schottky barriers formed between Au electrodes and ZnO also come into play by introducing a strong local electric field across the interface. Immediately after electron-hole pairs are generated upon UV illumination, they will be effectively separated by this local electric field, which reduces the recombination rate and increases the carrier lifetime and density. As a result, oxygen can be discharged and desorbed at a faster rate. Meanwhile, the SBH is decreased due to illumination so that more charge carriers can transport through the barrier region. These factors all lead to the enhanced sensitivity observed for Schottky-contact based ZnO

UV sensors.[48] When UV illumination is turned off, this local electric field can quickly restore the carrier distribution to its original status, overcoming the trapping effect, and hence lead to a shorter reset time.[48]

When strain is introduced into the system, the induced piezoelectric polarization charges can also effectively modulate the above processes, as shown by the schematics and band diagrams in Figure 5c. When tensile strain is applied (region in light yellow), negative polarization charges are induced at the top surface, promoting the oxygen adsorption/re-adsorption process, which contributes to the observed increased UV sensitivity and decreased reset time. Moreover, the induced negative piezopotential will raise the SBHs on both electrodes, resulting in further improvement to the UV sensing performance. On the other hand, when compressive strain is applied (region in light blue), the induced positive polarization charges at the surface will partially deplete the free electrons in the surface region, mitigating the oxygen adsorption/re-adsorption process, and hence decrease the UV sensitivity and increase the reset time. The positive ionic polarization charges at the semiconductor-metal interface can also lower the SBHs and further degrade the UV sensing performance.

In conclusion, flexible piezotronic device based on RF-sputtered piezoelectric semiconductor thin films has been investigated for the first time. The dominating role of piezotronic effect over geometrical and piezoresistive effect in the as-fabricated devices has been confirmed and the modulation effect of piezopotential on charge carrier transport under different strains is subsequently studied. Moreover, we also demonstrate that UV sensing capability of as-fabricated thin film based piezotronic device can be tuned by piezopotential, showing significantly enhanced sensitivity and improved reset time under tensile strain. It is prospected that piezoelectric semiconductor thin films can be an excellent alternative to their 1D counterpart for realizing piezotronic applications due to the technological compatibility with state-of-art microfabrication technology. Results demonstrated here broaden the scope of piezotronics and extend its potential applications in fields of sensors, flexible electronics, flexible optoelectronics, smart MEMS/NEMS and human-machine interfacing.

Acknowledgements

Research was supported by US Airforce, MURI, Department of Energy, Office of Basic Energy Sciences, Division of Materials Sciences and Engineering under Award DE-FG02-07ER46394, NSF (0946418), and the Knowledge Innovation Program of the Chinese Academy of Sciences (KJCX2-YW-M13).

Received: January 19, 2013
Revised: March 13, 2013
Published online:

[1] N. Izyumskaya, Y. Alivov, S. J. Cho, H. Morkoc, H. Lee, Y. S. Kang, *Crit. Rev. Solid State* **2007**, *32*, 111.
[2] H. Chen, C. Jia, C. Zhang, Z. H. Wang, C. S. Liu, *IEEE. Int. Symp. Circ. S* **2007**, 557.
[3] H. D. Espinosa, R. A. Bernal, M. Minary-Jolandan, *Adv. Mater.* **2012**, *24*, 4656.
[4] Z. L. Wang, X. Y. Kong, Y. Ding, P. X. Gao, W. L. Hughes, R. S. Yang, Y. Zhang, *Adv. Funct. Mater.* **2004**, *14*, 943.
[5] Z. L. Wang, J. H. Song, *Science* **2006**, *312*, 242.
[6] W. S. Su, Y. F. Chen, C. L. Hsiao, L. W. Tu, *Appl. Phys. Lett.* **2007**, 90.
[7] Z. L. Wang, *Adv. Mater.* **2012**, *24*, 4632.
[8] S. M. Sze, *Physics of semiconductor devices*, John Wiley & Sons, **1981**.
[9] Z. L. Wang, *J. Phys. Chem. Lett.* **2010**, *1*, 1388.
[10] Z. L. Wang, *Nano Today* **2010**, *5*, 540.
[11] Z. L. Wang, *Piezotronics and Piezo-Phototronics*, Springer, **2013**.
[12] W. Z. Wu, Y.G. Wei, Z.L. Wang, *Adv. Mater.* **2010**, *22*, 4711
[13] Q. Yang, W. H. Wang, S. Xu, Z. L. Wang, *Nano Lett.* **2011**, *11*, 4012.
[14] W. Z. Wu, Z. L. Wang, *Nano Lett.* **2011**, *11*, 2779.
[15] Y. F. Hu, Y. Zhang, L. Lin, Y. Ding, G. Zhu, Z. L. Wang, *Nano Lett.* **2012**, *12*, 3851.
[16] Y. Yang, W. X. Guo, Y. Zhang, Y. Ding, X. Wang, Z. L. Wang, *Nano Lett.* **2011**, *11*, 4812.
[17] Z. L. Wang, W. Z. Wu, *Angew. Chem. Int. Ed.* **2012**, *51*, 11700.
[18] J. Shi, M. B. Starr, H. Xiang, Y. Hara, M. A. Anderson, J. H. Seo, Z. Q. Ma, X. D. Wang, *Nano Lett.* **2011**, *11*, 5587.
[19] J. E. Allen, D. E. Perea, E. R. Hemesath, L. J. Lauhon, *Adv. Mater.* **2009**, *21*, 3067.
[20] D. E. Perea, E. R. Hemesath, E. J. Schwalbach, J. L. Lensch-Falk, P. W. Voorhees, L. J. Lauhon, *Nat. Nanotechnol.* **2009**, *4*, 315.
[21] Z. P. Huang, H. Fang, J. Zhu, *Adv. Mater.* **2007**, *19*, 744.
[22] E. M. Freer, O. Grachev, X. F. Duan, S. Martin, D. P. Stumbo, *Nat. Nanotechnol.* **2010**, *5*, 625.
[23] S. Acharya, A. B. Panda, N. Belman, S. Efrima, Y. Golan, *Adv. Mater.* **2006**, *18*, 210.
[24] Y. Zhang, Y. Liu, Z. L. Wang, *Adv. Mater.* **2011**, *23*, 3004.
[25] R. S. Muller, T. I. Kamins, M. Chan, *Device Electronics for Integrated Circuits*, Wiley, New York **2002**.
[26] J. Singh, *Semiconductor Optoelectronic: Physics and Technology*, McGraw-Hill, New York **1995**.
[27] J. McMurran, J. Kouvetakis, D. J. Smith, *Appl. Phys. Lett.* **1999**, *74*, 883.
[28] J. G. Lu, T. Kawaharamura, H. Nishinaka, Y. Kamada, T. Ohshima, S. Fujita, *J. Cryst. Growth.* **2007**, *299*, 1.
[29] S. Ilican, Y. Caglar, M. Caglar, *J. Optoelectron. Adv. Mater.* **2008**, *10*, 2578.
[30] Y. G. Wei, W. Z. Wu, R. Guo, D. J. Yuan, S. M. Das, Z. L. Wang, *Nano Lett.* **2010**, *10*, 3414.
[31] K. Tominaga, N. Umezu, I. Mori, T. Ushiro, T. Moriga, I. Nakabayashi, *Thin Solid Films* **1998**, *334*, 35.
[32] P. F. Carcia, R. S. McLean, M. H. Reilly, G. Nunes, *Appl. Phys. Lett.* **2003**, *82*, 1117.
[33] Y. F. Chen, D. M. Bagnall, Z. Q. Zhu, T. Sekiuchi, K. T. Park, K. Hiraga, T. Yao, S. Koyama, M. Y. Shen, T. Goto, *J. Cryst. Growth* **1997**, *181*, 165.
[34] W. C. Hughes, W. H. Rowland, M. A. L. Johnson, S. Fujita, J. W. Cook, J. F. Schetzina, J. Ren, J. A. Edmond, *J. Vac. Sci. Technol. B* **1995**, *13*, 1571.
[35] N. W. Emanetoglu, C. Gorla, Y. Liu, S. Liang, Y. Lu, *Mater. Sci. Semicond. Proc.* **1999**, *2*, 247.
[36] S. Nakamura, Y. Harada, M. Seno, *Appl. Phys. Lett.* **1991**, *58*, 2021.
[37] S. S. Lin, J. L. Huang, *Surf. Coat. Technol.* **2004**, *185*, 222.
[38] E. Mirica, G. Kowach, P. Evans, H. Du, *Cryst. Growth Des.* **2004**, *4*, 147.
[39] Z. Y. Gao, J. Zhou, Y. D. Gu, P. Fei, Y. Hao, G. Bao, Z. L. Wang, *J. Appl. Phys.* **2009**, 105.
[40] G. L. Dybwad, *J. Appl. Phys.* **1971**, *42*, 5192.
[41] S. Kazuta, Y. Cho, H. Odagawa, M. Kadota, *Jpn. J. Appl. Phys. 1* **2000**, *39*, 3121.
[42] Y. Gao, Z. L. Wang, *Nano Lett.* **2009**, *9*, 1103.

[43] R. W. Soutas-Little, *Elasticity*, XVI, 431; Dover Publications: Mineola, NY, **1999**.
[44] J. Zhou, P. Fei, Y. D. Gu, W. J. Mai, Y. F. Gao, R. Yang, G. Bao, Z. L. Wang, *Nano Lett.* **2008**, *8*, 3973.
[45] C. Soci, A. Zhang, B. Xiang, S. A. Dayeh, D. P. R. Aplin, J. Park, X. Y. Bao, Y. H. Lo, D. Wang, *Nano Lett.* **2007**, *7*, 1003.
[46] K. Keem, H. Kim, G. T. Kim, J. S. Lee, B. Min, K. Cho, M. Y. Sung, S. Kim, *Appl. Phys. Lett.* **2004**, *84*, 4376.
[47] Q. H. Li, T. Gao, Y. G. Wang, T. H. Wang, *Appl. Phys. Lett.* **2005**, 86.
[48] J. Zhou, Y. D. Gu, Y. F. Hu, W. J. Mai, P. H. Yeh, G. Bao, A. K. Sood, D. L. Polla, Z. L. Wang, *Appl. Phys. Lett.* **2009**, 94.